KSCE Journal of Civil Engineering (2022) 26(2):727-740
DOI 10.1007/s12205-021-1835-6

pISSN 1226-7988, eISSN 1976-3808
www.springer.com/12205

Structural Engineering

Experimental Study of Evolution of Fracture Process Zone in Dam Concrete under Cyclic Loading Using Digital Image Correlation

Xudong Chen[a], **Shengtao Li**[a], **and Xiyuan Cheng**[a]

[a]*College of Civil and Transportation Engineering, Hohai University, Nanjing 210098, China*

ARTICLE HISTORY

Received 13 October 2020
Accepted 22 August 2021
Published Online 28 October 2021

KEYWORDS

Dam concrete
Cyclic load
Fracture process zone
Digital image correlation
Rate effect

ABSTRACT

In this paper, three-point bending tests were carried out o investigate the post-peak cyclic loading behavior of dam concrete under two loading rates. The fracture parameters, residual load capacity, cyclic modulus, dissipated energy, and deformation recovery were presented and analyzed. The analysis was made to understand the evolution of fracture process zone (FPZ) under post-peak cyclic loading for dam concrete by utilizing digital image correlation (DIC) technique. The results showed while the dam concrete under a higher loading rate showed an increase in maximum load, it is not necessarily the same for post-peak bearing capacity. The specimens with higher post-peak bearing capacity had higher residual stiffness, higher dissipation energy, and higher Crack Mouth Opening Displacement (CMOD) reversibility under cyclic loading. The FPZ development was investigated quantitatively, and the extension and retraction of its tip were observed. Moreover, it was found that the FPZ in specimens with higher residual stiffness developed more slowly, and FPZ had a more significant retraction rate during unloading for the specimens with higher residual bearing capacity.

1. Introduction

Concrete dams are critical infrastructure with flood control, drought resistance, power generation, and other functions. Because of the demand for clean energy, the construction of dams is also growing. By the end of the 20th century, more than 40,000 large dams have been built or are under construction all over the world (World Commission on Dams, 2000). At present, there are more than ten concrete dams over 200 m high in China (Song et al., 2016). The safety of concrete dams is a very critical issue, whereas concrete dams may be damaged in different scales due to earthquake, temperature changes, and sudden loads in use (Leger et al., 1993; Ghrib and Tinawi, 1995; Fedele et al., 2005; Ardito et al., 2008; Tatin et al., 2015). The initiation, combination, and propagation of internal micro-cracks form the fracture process zone (FPZ) at the crack tip (Wecharatana and Shah, 1983; Nomura et al., 1991; Hu and Wittmann et al., 1992; Hu and Duan, 2004). The development of FPZ leads to macro cracks, which threatens the safety of concrete structures. Many mechanical properties of concrete are mainly attributed to the properties of FPZ, including non-linear behavior of concrete, post-peak strain softening, toughening after the main crack, sliding friction of aggregate boundary, etc. Therefore, it is critical to study the FPZ behavior and failure evolution of dam concrete.

The mechanical properties of dam concrete are pretty different from ordinary concrete, mainly due to the influence of large-size aggregate. Previous studies showed the necessity of experimental researches on dam concrete for its particular mechanical property (Mihashi et al., 1991; Saouma et al., 1991; Wu et al., 2001; Li et al., 2004; Deng et al., 2008; Elices and Rocco, 2008; Li et al., 2019a). Dam concrete is usually subjected to cyclic load due to seasonal changes in temperature, environment, and water level (De Sortis and Paoliani, 2007; Mata, 2011). The previous studies staying in the basic compression and tension tests might not be enough to describe the characteristics of dam concrete. It is necessary to investigate the behavior of the dam concrete at the post-peak stage to understand the deterioration mechanism of dam concrete under cyclic loads (Reinhardt and Cornelissen, 1984; Bhattacharjee and Leger, 1993; Ren et al., 2007).

On the other hand, the monitoring of FPZ is an issue of great concern to researchers (Cedolin et al., 1983). DIC is a very effective and convenient non-destructive measurement technology. With

CORRESPONDENCE Xudong Chen cxdong1985@hotmail.com College of Civil and Transportation Engineering, Hohai University, Nanjing 210098, China

the development of this technology, it has been used to measure the deformation of many engineering materials, which provides the possibility for the observation of FPZ (Choi and Shah, 1997; Poissant and Barthelat, 2010; Safavizadeh and Kim, 2017; Guo et al., 2019). Choi and Shah (1997) tried to use DIC to observe the FPZ of concrete a long time ago. But at that time, the DIC technique was not mature. There was a problem of measurement accuracy, and because of the limitation of the calculation ability, the description of FPZ development could not be realized. With the development of DIC, researchers began to use DIC to study FPZ again. Skarzynski and Tejchman (2013) have tried to use DIC to characterize FPZ of plain concrete beams, and FPZ width was studied. More and more researchers begin to pay attention to the variation of FPZ length, which is becoming a hot issue (Wu et al., 2011; Bhowmik and Ray, 2019; Miao et al., 2020). But at present, there is no standard method to determine the length of FPZ, and few methods can quantify the dynamic development of FPZ.

Based on the authors' previous work, this paper realized a quantitative study on FPZ development in post-peak cyclic loading condition (Li et al., 2020). Three-point bending tests of dam concrete were carried out first, and the post-peak behavior was studied. Two different incremental displacement rates were adopted to study the effect of loading rates on the load capacity of dam concrete. The peak bearing capacity, post-peak residual bearing capacity, cyclic modulus, dissipated energy, and residual crack opening displacement were analyzed. The typical strain images under cyclic loading, the variation of strain, and displacement at the crack with loading cycle were also investigated using DIC. The result will contribute to the understanding of the crack growth mechanism of dam concrete.

2. Experimental Work

2.1 Materials and Specimens

In this paper, two kinds of dam concrete, including full-graded and three-graded concrete, are studied. The mixing composition of full-graded dam concrete and three-graded concrete is given in Table 1. The commercially available ordinary Portland cement is used in the mixtures. The mixture contains fly ash and the high-performance polycarboxylic water reducer as additives to achieve good workability. The coarse aggregate is 20 – 150 mm natural granite, and the fine aggregate size distribution accord with the ASTM C33 (2003) specification. The specific proportion is shown in Table 1.

Two kinds of specimens were poured during the test. The first kind is the full-graded concrete beam with a 450 * 450 * 1,700 mm size, and the second one is the three-graded concrete beam with a 300 * 300 * 1,100 mm size. Concrete were mixed in a drum mixer. Then the fresh concrete were poured into the prefabricated wood molds in four stages. Each concrete pouring is one fourth of the mold volume. Vibrators were used to make concrete dense. The steel sheet was inserted in the mid-span of the specimen, and the steel sheet was pulled out after casting to form the notch. The notch width was about 2 mm. The notch-to-height ratio of the specimens was 0.4. The specimens were removed from the mold two days after casting.

2.2 Testing Procedure and Setup

The experimental setup is shown in Fig. 1. A 500 kN hydraulic servo MTS testing machine was used for the three-point bending test. The loading mode of displacement control or force control can be chosen according to different test requirements. All specimens were loaded to the peak load first and then cyclically unloaded and loaded after the peak load. A clamp extensometer was set in the mid-span of the specimen to measure the opening displacement of the prefabricated crack mouth. Two steel cylinders supported the two ends of the beam, one of which was fixed, and the other can move horizontally. The depth-span ratio was 0.3 in this study. Two digital cameras were fixed in front of concrete beams using tripods to focus on the fracture ligament zone of dam concrete, i.e., the area above the notch. Two LED lights were installed to obtain a higher quality speckle image. The

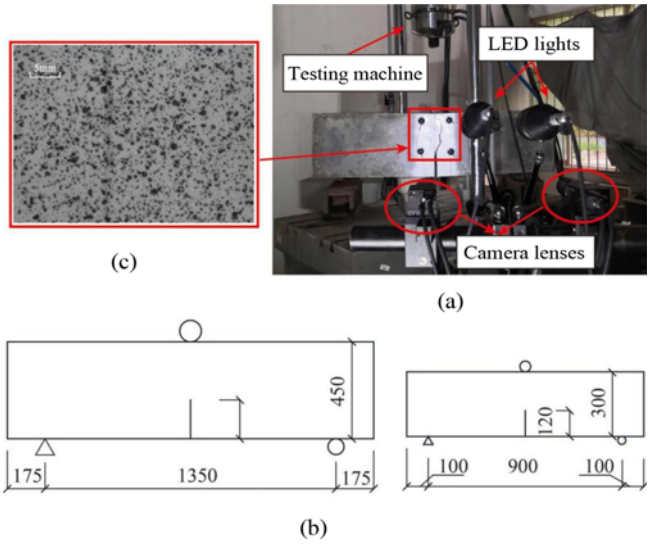

Fig. 1. Schematic Diagram of Experimental Setup: (a) Test Arrangement with the DIC Settings, (b) The Closed View of Speckle Pattern, (c) Geometric Details of Full-Graded Concrete and Three Graded Concrete Specimens

Table 1. Mix Ratio of Dam Concrete Specimens (kg/m^3)

Type	Cement	Fly ash	Sand	Small stone (20 mm)	Medium stone (40 mm)	Large stone (80 mm)	Extra-large stone (120 mm)	Water	Water reducer
Full-graded	150.8	81.2	591	400	320	400	480	115	2.66
Three-graded	210	90	711	375	375	500	-	138	6.27

resolution of the cameras was 2,448 * 2,048. The camera triggered shooting with the start of the testing machine and automatically collected photos with a preset rate until the specimen was destroyed. In the image analysis, the size of the calculation subset was 20 × 20 pixels, while the step size was set as 7 pixels to improve the spatial resolution. The strain field was calculated by using the strain window of 5 × 5 pixels. First, the normalized cross-correlation (NCC) method was adopted, and then a non-linear optimization algorithm was used to refine the results. The accuracy of DIC used in this paper has been verified in previous studies of the authors (Li et al., 2019b). According to our calibration, the accuracy of displacement measurement is 10 μm in this study.

The loading process scheme consists of two parts. The concrete specimen is prone to lose stability in the loading process once it enters the post-peak stage. Using displacement control can ensure the specimen enters the post-peak stage without instability. Hence, the first part was set to be controlled by displacement. In the unloading process, the force control mode was adopted, which is most frequently used. In addition, two rates with ten times difference were selected to study the effect of loading rate, which were 0.001 and 0.01, respectively. The selection of rate refers to previous research (Bažant and Gettu, 1992). Because the size of the full-graded concrete beam is different from that of the three-graded, their displacement settings should be different in the stage of displacement control. The specific displacement control was determined by the monotonic loading test carried out in advance. In this paper, the crack mouth opening displacement (CMOD) of the full-graded concrete was first loaded to 0.2 mm and then unloaded to start the first loading cycle, and the CMOD of the three-graded concrete was loaded to 0.15 mm to start the first loading cycle. For full-graded concrete, the CMOD was increased by 0.1 mm per loading cycle because of its larger ultimate deformation value. While for three-graded concrete, unloading began after increasing CMOD by 0.05 mm at each loading cycle. For the unloading process, force control was adopted to unload the beam to 0.1 kN at a fixed decreasing rate of 1 kN/s. Fig. 2 shows the schematic diagram of the loading and unloading process.

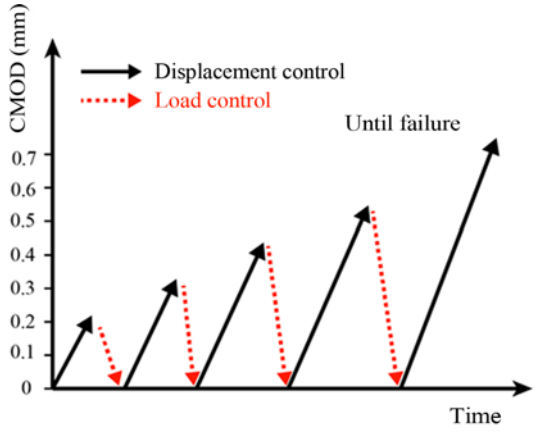

Fig. 2. Diagram of Loop Loader for Full-Graded Concrete

3. Experimental Results

3.1 Load-Displacement Curves for Post-peak Cyclic Experiments

The MTS testing machine was used to carry out post-peak cyclic tests on dam concrete. FDC-1 indicates the loading rate of 0.01 mm/s for full-graded dam concrete, while FDC-2 represents the loading rate of 0.001 mm/s, TDC-1 the loading rate of 0.01 mm/s for three-graded dam concrete, and TDC-2 the loading rate of 0.001 mm/s. The tests were repeated three times under each condition, and the results are similar. Fig. 3 shows the typical load-CMOD responses of dam concrete in flexural tests. From Fig. 3, it can be observed that the load-bearing capacity of dam concrete will drop suddenly after the peak load appears, and the inclination angle of the hysteretic loop is on the descent with the increase of loading cycles. The increase in compliance indicates the stiffness decrease of the specimen and the crack growth (Swartz and Go, 1984).

The average maximum load P_u of specimens and the corresponding $CMOD_c$ are listed in Table 2. The recovery rates of the first and second cycles of the specimens are also provided in Table 2. The double K fracture parameters of each specimen are calculated by using the load-CMOD curve. The formula defines the fracture parameters of double-K fracture criterion in three-point bending test in reference (Xu and Reinhardt, 1999):

$$K = \frac{3PS}{2h^2t}\sqrt{a}\,f(\alpha), \tag{1}$$

in which a is the crack length, α the crack height ratio, P the vertical load, S the span of the beam, h the height of the beam, and t the thickness of the beam. On the other hand, because in this paper, the span-height ratio β is three rather than the standard value four, so it is different from the standard formula, which is (Guinea et al., 1998):

$$f_\beta(\alpha) = \frac{p_\infty(\alpha) + \frac{4}{\beta}[p_4(\alpha) - p_\infty(\alpha)]}{(1-\alpha)^{3/2}(1+3\alpha)}, \tag{2}$$

in which $p_\beta(\alpha)$ are cubic polynomials, and the expressions for $\beta = 4$ and $\beta = \infty$ are as follows:

$$p_4(\alpha) = 1.9 + 0.41\alpha + 0.51\alpha^2 - 0.17\alpha^3, \tag{3}$$

$$p_\infty(\alpha) = 1.99 + 0.83\alpha - 0.31\alpha^2 + 0.41\alpha^3. \tag{4}$$

The initial fracture toughness K_{ini} was obtained by using $a = a_0$, and $P = P_{ini}$. a_0 was the length of the notch. In the present study, P_{ini} was determined by the graphical method using the points where the non-linearity starts in the P-CMOD curve listed in Table 2. At the same time, the critical crack toughness K_{un} was calculated by using $a = a_c$ and $P = P_u$. The value of equivalent elastic crack-length in three-point bending specimen was calculated by the formula in reference (Shah, 1990):

$$a_c = \frac{Ec_u h^2 t}{6SV_\beta(\alpha)}, \tag{5}$$

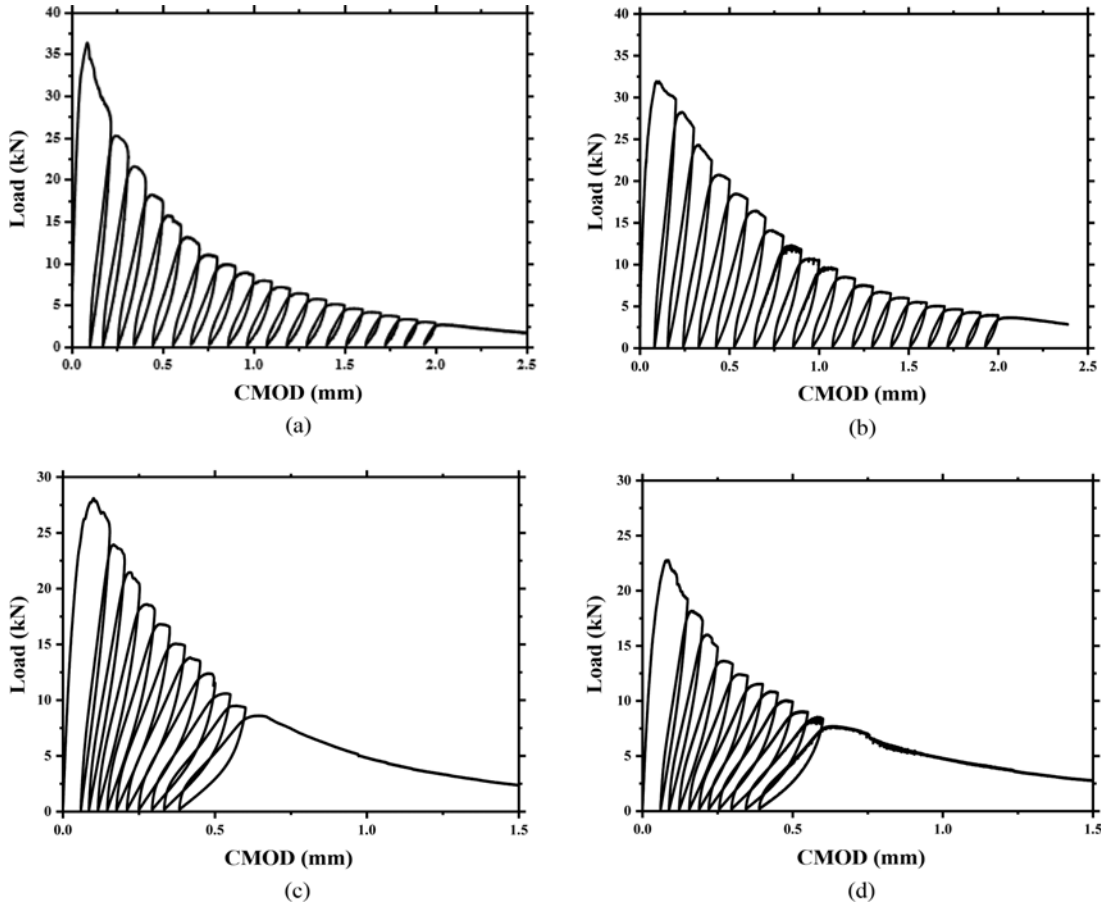

Fig. 3. The Load-CMOD Responses of Specimens with Different Gradations: (a) FDC-1, (b) FDC-2, (c) TDC-1, (d) TDC-2

Table 2. Experimental Results of Fracture Parameters and Load and CMOD Measurement

	Loading rate (mm/s)	Maximum aggregate size (mm)	P_u (kN)	P_{ini} (kN)	Load recovery of 1st cycle (kN/%)	Load recovery of 2st cycle (kN/%)	$CMOD_u$ (μm)	a_c (mm)	K_{ini} (MPa $\sqrt{m}$)	K_{un} (MPa $\sqrt{m}$)
FDC-1	0.01	120	36.3	31.06	25.16/69.3%	21.49/59.2%	86	222.6	0.68	0.91
FDC-2	0.001	120	31.9	22.58	28.23/88.5%	24.31/76.2%	109	246.0	0.54	0.94
TDC-1	0.01	80	28.0	23.42	23.94/85.5%	21.45/76.6%	100	145.8	0.88	1.19
TDC-2	0.001	80	22.8	16.19	18.19/79.8%	16.05/70.4%	86	147.4	0.65	0.99

in which $c_u = CMOD_u / P_u$, and the expressions for $V_\beta(\alpha)$ are as follows (Zhang et al., 2009):

$$V_\beta(\alpha) = 0.8 - 1.7\alpha + 2.4\alpha^2 + \frac{0.66}{(1-\alpha)^2} + \frac{4}{\beta}(-0.04 - 0.58\alpha + 1.47\alpha^2 - 2.04\alpha^3), \quad (6)$$

and the modulus of elasticity can be obtained from the P-CMOD curve according to the following formula (Shah, 1990):

$$E = \frac{6Sa_0V_\beta(\alpha_0)}{C_i h^2 t}, \quad (7)$$

where $c_i = CMOD_i / P_i$, $CMOD_i$ and P_i can be obtained respectively from the CMOD and P values of a point in linear elasticity stage, $\alpha_0 = (a_0 + h_0)/(h + h_0)$, h_0 is the thickness of the clip gauge holder.

For full-graded dam concrete, when the loading rate is 0.001 mm/s, the load-bearing capacity P_u is 31.9 kN, and the $CMOD_c$, i.e., crack mouth opening displacement at peak load, is 90 μm. When the loading rate increases to 0.1 mm/s, the maximum load-bearing capacity increases by 14%. For three-graded concrete, when the rate increases to 0.1 mm/s, the P_u increases by 23%, and the corresponding $CMOD_c$ is 100 μm. It can be seen that for dam concretes, the increase of loading rate will increase the maximum load-bearing capacity accordingly, which is consistent with the results of previous researches (Zhang et al., 2009). However, for the post-peak performance, the dam concrete does

not show the same trend with the rate as shown in Table 2. Under the loading rate of 0.001 mm/s, the peak load of FDC-2 in the first cycle after peak reached 28.2 kN, which exceeded the residual bearing capacity of FDC-1. It is still the same result in the next loading cycles. On the contrary, the residual bearing capacity of TDC-1 is still higher than that of TDC-2 in next loading cycles. In addition, it is noticed that the specimen with a higher maximum load has a larger initial fracture toughness. At the same time, the specimen with higher residual bearing capacity has a larger critical fracture toughness. This result indicates that the effect of the loading rate on mechanical behavior in the post-peak field is different from that before the peak. The main factor affecting the residual bearing capacity in the post-peak field is not the loading rate but maybe the development degree of the cracks after the peak. From the above analysis, it can be seen that the increase of loading rate has a more significant impact on the peak load of dam concrete, but its impact on the load capacity in the post-peak field is not apparent. The post-peak load-bearing capacity of specimens may be more affected by other factors such as aggregate distribution and aggregate size, which will be analyzed in the DIC results in the following paper.

3.2 Cyclic Modulus

The hysteretic loops formed by loading-unloading processes are obtained from the load and displacement (P-CMOD) curve. They are analyzed locally to study the post-peak performance of dam concrete. When the concrete beams were subjected to the cyclic load, permanent deformation originates from the destruction of the bond between aggregate and cementitious material, and the extension of micro-cracks results in the macroscopic plastic deformation and stiffness reduction of concrete. The flexural behavior of dam concrete under the post-peak cyclic loading condition is first evaluated by its cyclic modulus. Initial tangential

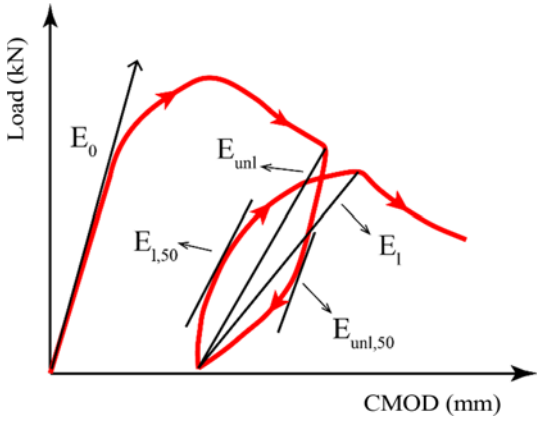

Fig. 4. Schematic Diagram of Cyclic Modulus

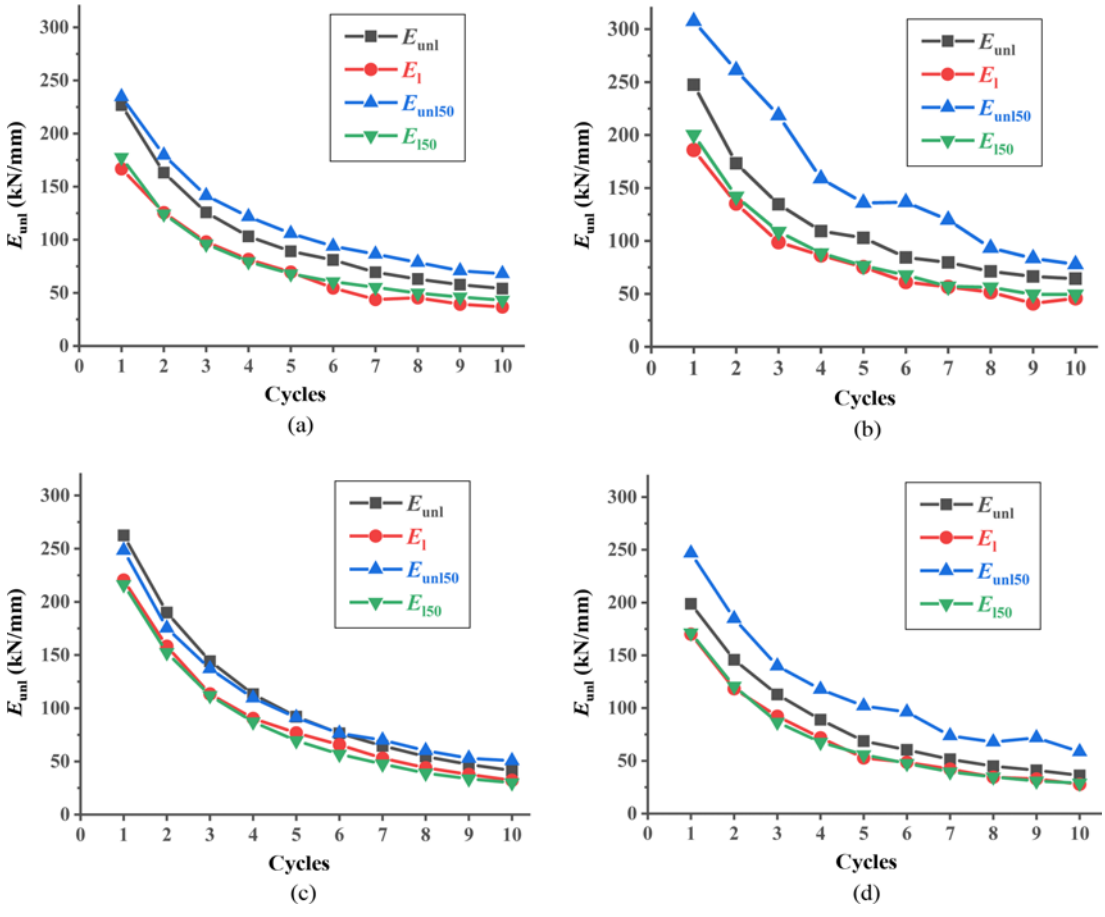

Fig. 5. Variations of Different Types of Cyclic Modulus: (a) FDC-1, (b) FDC-2, (c) TDC-1, (d) TDC-2

modulus E_0 corresponds to the slope at the beginning of the P-CMOD curve, as shown in Fig. 4. Four cyclic moduli are applied to evaluate the deformation characteristics of dam concrete beams in each loading cycle. Among them, E_{unl} is determined by the slope of the line connecting the beginning point and the endpoint of the unloading process, E_l is the slope of the line connecting starting point and endpoint of the loading process, $E_{unl,50}$ and $E_{l,50}$ represent the slope of the tangent at the midpoint of the unloading- and the loading process, respectively.

The cyclic modulus change is associated with crack growth and can reflect the damage for a given loading condition in concrete. Fig. 5 shows the evolution of the cyclic modulus with the loading cycle. The cyclic moduli in the unloading process are noticed to be greater than those in the loading process. It is particularly interesting to find that the rate change influences the unloading process rather than the reloading stage since we observed that the values of the $E_{l,50}$ and E_l are close in both loading rates. In contrast, the values of the E_{unl} and $E_{unl,50}$ have a large difference under the lower loading rate. The reason could be that the non-linear post-peak behavior of concrete is time-dependent. In the present study, the reloading and unloading process duration is similar for the higher loading rate. In contrast, the time in the unloading process is much longer than the time consumed in the reloading process for the lower rate. The slower reloading process may lead to a more complete formation and growth of micro-cracks during the crack propagation in concrete, making the internal non-linear behavior continuously enhanced and thus results in a greater difference between the cyclic modulus.

In the present study, the normalized cyclic modulus is defined as E_l/E_0 and is calculated for each cycle. It is observed that the huge damage is caused during the first loading process to the peak, after which the normalized moduli drop down sharply to a value all lower than 50%. This result marks that the stiffness has decreased with the microcracking activity and the bond failure between the cement mortar and coarse aggregate in concrete. Further, the normalized modulus is observed to have a rapid decrease in the first few cycles. It shows that the specimen has the main stiffness decrease during the first few cycles, which may be due to the rapid growth of the micro-crack in concrete. In addition, it should be noticed that the normalized modulus is found to be consistent with the residual load capacity, wherein the values of FDC-2 are higher than FDC-1, and the values of TDC-1 are greater than TDC-2. This result shows that the specimens with high residual capacity seem to have higher residual stiffness.

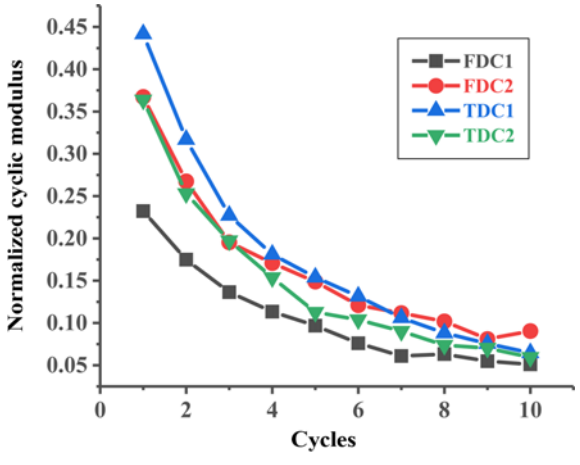

Fig. 6. Development of Normalized Cyclic Modulus of Dam Concrete

3.3 The Dissipated Energy

Figure 7 illustrates the energy released during unloading and input during loading in each hysteresis loop. Part S1 corresponds to the elastic energy released in the cycle, while S2 is the dissipated energy in the cycle. It is noticed that the absorbed energy is always more than the released energy, which shows that a part of the energy is dissipated. During the unloading and reloading process in concrete beams, the close and re-opening of cracks occur with new-crack formation, growth, and friction between interfaces. The energy is lost in these ways and cannot be used to return the material to its original shape. This energy difference is the energy dissipated by the material due to the load cycle (Ghuzlan and Carpenter, 2006). Local analysis of dissipated energy is performed in each loading cycle. The energy dissipation occurring during loading and unloading of dam concrete can be expressed by Eq. (8):

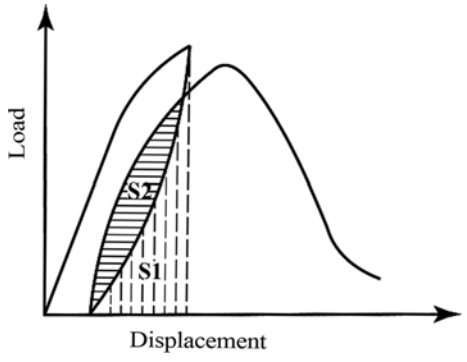

Fig. 7. A Schematic Diagram of Cyclic Dissipated Energy

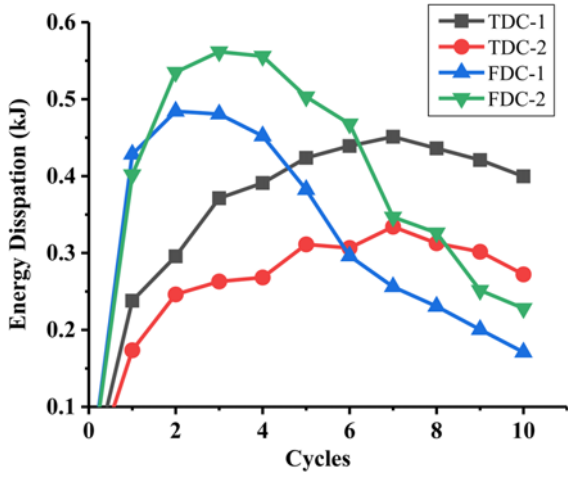

Fig. 8. Variations of Dissipated Energy in Each Cycle

$$W_i = \int_i w(x)dx \quad (8)$$

where W_i represents the energy dissipation in the i-th loading cycle and $w(x)$ is the P-CMOD response of the i-th loop curve.

Figure 8 shows the relationship between dissipated energy and the cycle number. It can be seen that the energy dissipation of all specimens shows prominent two-stage characteristics. In the first stage, the energy dissipated in each cycle is rising continuously. Then it enters the second stage, in which the dissipated energy decreases with the increase of the loading cycles. The first stage indicates that cracks develop continuously in the first few loading cycles. The intensive cracking takes place in more areas in this stage, which causes the softening behavior of concrete. A large amount of strain energy is stored in concrete with local strain concentration in this stage. After the FPZ in concrete has been fully developed at the end of the first stage, the newly formed concentration zone decreases in each cycle, leaving a crack opening and fracture, the main activity occurring in concrete and the bearing capacity continuously decreasing.

The dissipated energy of full-graded concrete is generally higher since it has a larger fracture area. The value of the dissipated energy reaches a peak in the second to third cycle, which indicates that the accumulation of damage in concrete is mainly concentrated in these initial loading cycles. The maximum dissipation energy of full-graded concrete at the higher loading rate is 0.49 kJ. When the loading rate decreased to 0.001 mm/s, the maximum dissipation energy of full-graded concrete is 0.56 kJ. The dissipated energy of the three-graded concrete increases with the cycles, and it reaches the maximum value at around the seventh cycle. This result shows the relatively stable damage accumulation process of three-graded concrete, which may due to the smaller incremental CMOD value in each cycle. The maximum dissipated energy of three-graded concrete at 0.001 mm/s and 0.01 mm/s loading rates is 0.45 kJ and 0.33 kJ, respectively. It should be noticed that the dissipated energy of FDC-2 is larger than that of FDC-1. In comparison, the energy of TDC-1 is larger than that of TDC-2, which shows that the specimen with a larger residual bearing capacity after the peak has larger dissipation energy.

3.4 Displacement Recovery Performance

The clamp extensometer can obtain the CMOD of the specimens at the mid-span of the beams. A local analysis is made from the post-peak loading cycles to study the reversibility of dam concrete. The irreversibility of displacement is usually used to reflect the plastic damage. The failure of the bond between aggregate and matrix is the first permanent deformation. After the failure, the cracks begin to grow, which leads to permanent macroscopic deformation besides elastic deformation. In this section, displacement recovery is used to characterize the post-peak recovery performance of dam concrete. The reversibility is defined by the recovery ratio, which can be expressed by Eq. (9):

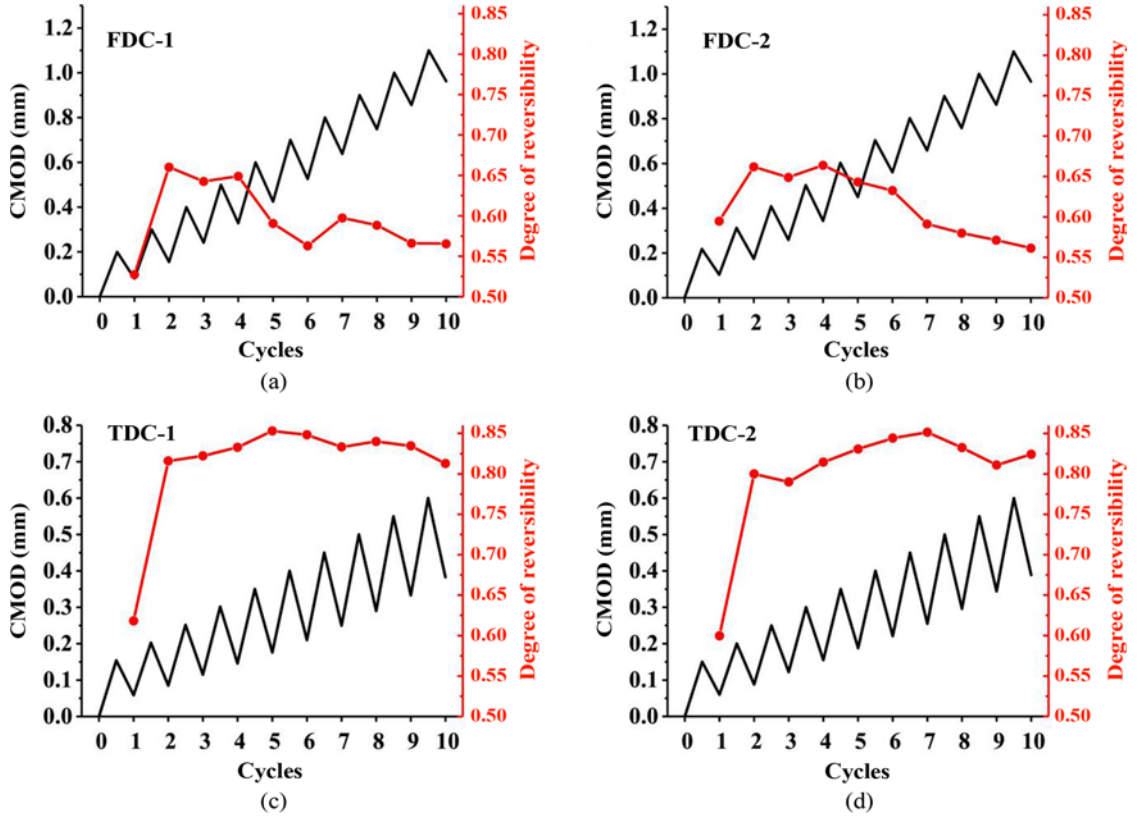

Fig. 9. History of Crack Opening Displacement and Response Ratio of Specimens: (a) FDC-1, (b) FDC-2, (c) TDC-1, (d) TDC-2

$$R = \frac{CMOD_{\max} - CMOD_{residual}}{CMOD_{\max} - CMOD_0}, \quad (9)$$

$CMOD_0$ is the value of $CMOD$ at the point where the reloading begins, $CMOD_{\max}$ the largest displacement in each loading cycle, and $CMOD_{residual}$ the corresponding CMOD value at the point where the force is the smallest after unloading. Fig. 9 shows the variations of CMOD and degree of reversibility with the loading cycles. It can be observed that the degree of the reversibility shows the same result as the cyclic modulus after the first cycle, wherein it remains a very low value which is less than 60%, indicating that there is serious damage in concrete after loading to the peak value. Interestingly, the development of reversibility is observed to have a similar trend with dissipation energy. The reversibility of the full-graded concrete decreases after reaching the maximum in the first few cycles. In contrast, the three-graded concrete continues to increase until the later cycles. It is found that the recovery ratio of FDC-2 is generally higher than FDC-1, while that of TDC-1 is higher than that of TDC-2. This result indicates that the concrete with higher residual load capacity may has higher reversibility.

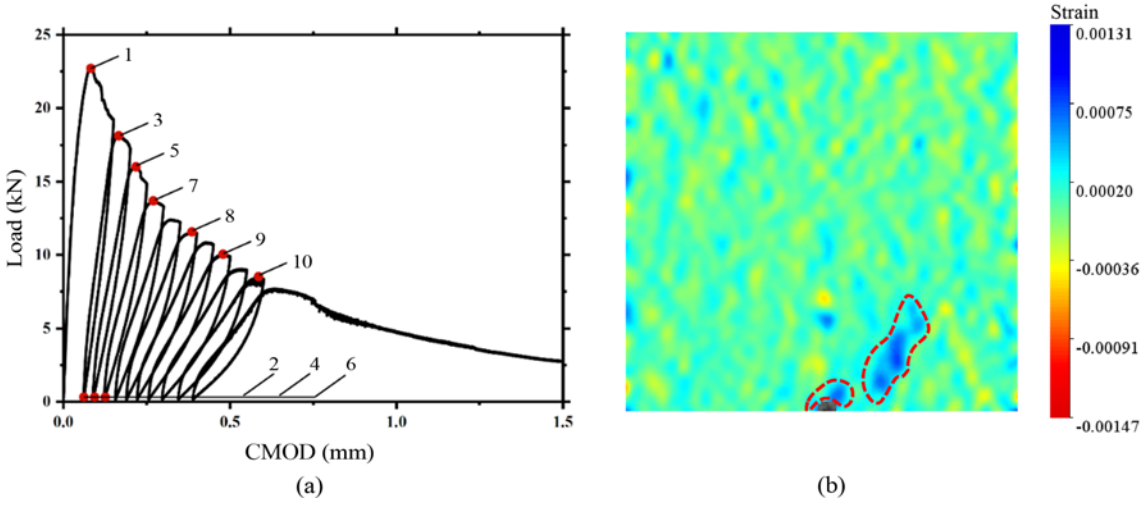

Fig. 10. Corresponding Loading Points for DIC Observation: (a) Corresponding Loading Points of TDC-1, (b) Contours of exx when FPZ Appears

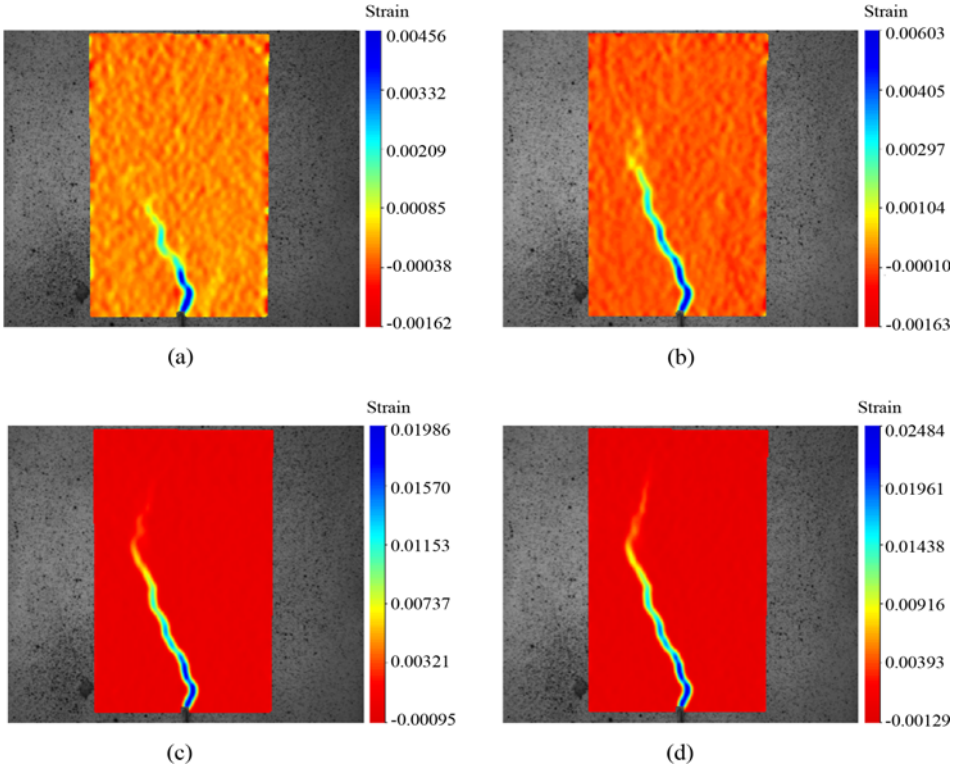

Fig. 11. Horizontal Strain Contours of TDC-1 Specimen: (a) Peak Load, (b) The First Valley Load, (c) The Third Valley Load, (d) The Fourth Peak Load

3.5 DIC Observation

3.5.1 Horizontal Strain Contour

In the three-point bending experiment, the crack tip of the specimen mainly generates intensive deformation in the horizontal direction. The deformation in this zone is much larger than that in other areas because of the concentrated micro-cracks. TDC-1 was selected as a typical example to show the variation of horizontal strain concentration in dam concrete with cyclic loads. The variation of the horizontal strain was investigated by selecting the peak and valley points of the loading cycles as shown in Fig. 10(a) to observe the fracture process. As shown in Fig. 10(b), DIC results show that a prominent strain concentration area can be observed in the contour when the specimen reaches 83% of maximum load. This result indicates that the FPZ emerged in this area.

The horizontal strain contours at some load points given in Fig. 10(a) are shown in Fig. 11. Figs. 11(a) and 11(b) display the strain contours of TDC-1 at the first peak load and the first valley load, respectively. From Figs. 11(a) and 11(b), it can be seen that the strain concentration area has developed long, and after the first unloading procedure, the strain concentration area developed further. Figs. 11(c) and 11(d) shows the conditions correspond to the third valley load and the fourth peak load marked in Fig. 10, respectively. It was noticed from Fig. 11(d) that at the peak of the fourth cycle, the FPZ changed its growth direction in the development process and began to develop toward the right side, which indicates that the crack may has encountered large aggregates in the development process. The sudden direction change of crack development like this often occurs in other specimens.

3.5.2 Evolution of the Crack Opening Displacement and Strain

The parameters discussed above provide a global view of the mechanical response, but they cannot describe the local damage. DIC analysis first aims to clarify the local deformation under the cyclic loading. The strain and the crack opening displacement (COD) in the strain concentration area at 30 mm above the notch tip are analyzed in Fig. 12. The strain distributions above the crack tip corresponding to the different loading points 1 – 6 in Fig. 10 are presented. From Fig. 12(a), it can be seen that the horizontal strain, i.e., *exx*, reaches the peak value at the horizontal coordinate 80 mm, which indicates that the strain concentration occurs in the coordinate range of 75 mm – 85 mm. At loading point 1, the peak strain is small, and with a period of development, the residual strain shows that there has formed a larger irreversible deformation at point 2. In the second and third loading cycles, it can be seen that the strain has greatly increased at points 3 and 5, and a certain strain recovery has occurred after the unloading at points 4 and 6. Fig. 12(b) displays the horizontal displacement at the selected location. There is a huge difference in the values around the coordinate 80 mm, while that in other locations is much smaller. The location where the rapid change occurs is taken as the position where the crack grows. The crack width can be obtained by calculating the displacement difference between the right side and the left. It is observed that the crack is very small at the maximum peak load as the calculated crack width at this time is less than 20 μm. After the second reloading procedure, the crack width expands to 87 μm, and it reduces to 69 μm after unloading. The recovery rate of crack opening width is 21%. After the third reloading procedure, the crack width is 137 μm, and it returns to 113 μm after unloading with a recovery rate of 17.5%. The displacement recovery rates of CMOD in the same period were 56% and 51%, respectively. It is interesting to find a large difference between the displacement recovery rate of CMOD and that of local crack width above the notch tip. This can be explained by the fact that CMOD provides a global view of the mechanical behavior, while the observation by DIC in the stress-transferring area can provide a local analysis of the deformation. DIC results suggest that the recovery rate of crack opening displacement above the notch tip is lower than that of CMOD, which indicates that the displacement at this location is mainly caused by the plastic deformation of concrete.

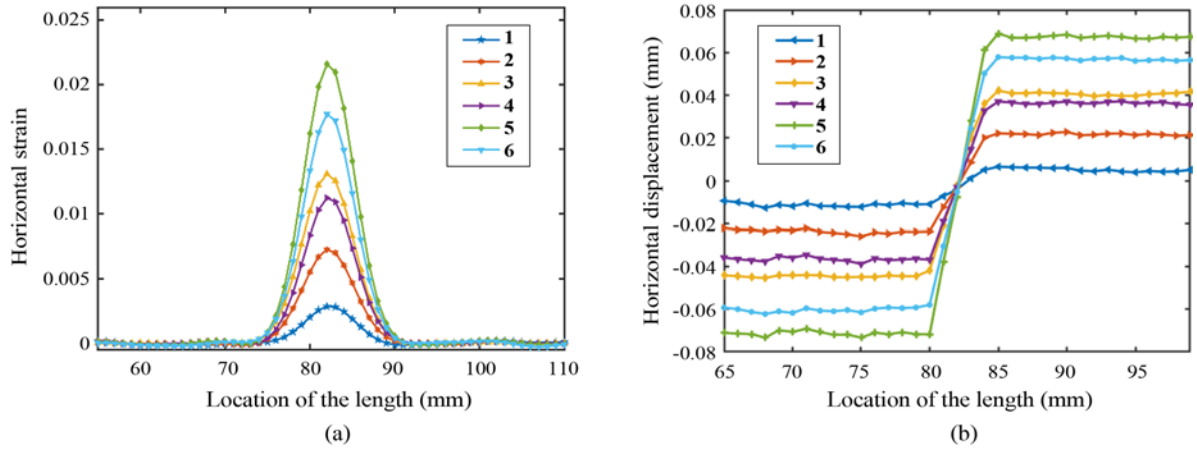

Fig. 12. Strain and Displacement along a Horizontal Direction at 30 mm above the Crack Tip under Different Cyclic Loads: (a) Variation of Horizontal Strain at Different Loading Points, (b) Variation of U_x at Different Loading Points

3.5.3 FPZ Determination and Its Evolution in Loading Cycles

As observed above in Figs. 11 and 12, due to the presence of large micro-crack concentrated in FPZ, the deformation in this zone is obviously more extensive than that in the non-cohesive crack zone, which can be observed by DIC. On the other hand, with the development of DIC technology, many researchers put forward corresponding improvement methods, such as smoothing the displacement first and then calculating the strain, and these mechanisms can greatly reduce the displacement noise and increase the strain accuracy (Sutton et al., 1991; Tong, 1997; Wang et al., 2002). Therefore, the FPZ has the basis to be determined by the characteristic of the strain field. The following is a brief introduction to determining FPZ, and the exact method can be found in Li et al. (2020). Fig. 13(a) shows the processed horizontal strain contour of the specimen during the test with the positioning process of FPZ. First, an appropriate strain threshold (T), which equal to 0.004, was set to distinguish the FPZ from the other normal area based on the resolution and environment noise. As shown in Figs. 13(b) – 13(d), when a smaller strain threshold is used, more strain concentration areas can be observed, and the heterogeneity of the specimen can be more obvious. But in this case, the observed FPZ may be easily affected by environmental noise. Many areas aren't screened out and affect the observation of the FPZ, so a larger strain threshold should be chosen to observe the specimen surface. Appropriately increasing the strain threshold makes the FPZ explicit, providing enough accuracy and convenience for observation. And it should be noticed from Figs. 13(b) – 13(d) that, with the increase of threshold value, the surrounding interference area disappeared rapidly, whereas the length of FPZ had hardly changed. This result shows that FPZ can be well presented under an appropriate threshold when the environmental noise is primarily removed. After removing the noise from the strain contours of the specimens, a MATLAB program has been written to automatically obtain the length from the notch tip to the FPZ tip, and statistical analyses are applied to observe the length variation during the test.

The FPZ development can be expressed by the FPZ length ratio, that is, the length of FPZ divided by the length of the fracture ligament. Fig. 14 shows the comparison of the force with the variation in the FPZ length ratio of specimens. It can be seen in the plots that the FPZ length fluctuates obviously with the change of load and follows the same trend as the load in 10 cycles of the whole loading process. It is observed from the plots that the lowest process zone length occurs at the minimum force, and the highest length takes place at the peak force in each force cycle. This is because unloading would make part of the micro-cracks in FPZ close. In addition, as can be seen in Fig. 14, in the initial loading cycles, the FPZ length raises and drops down greatly during loading cycles, whereas, as the number of cycles increases,

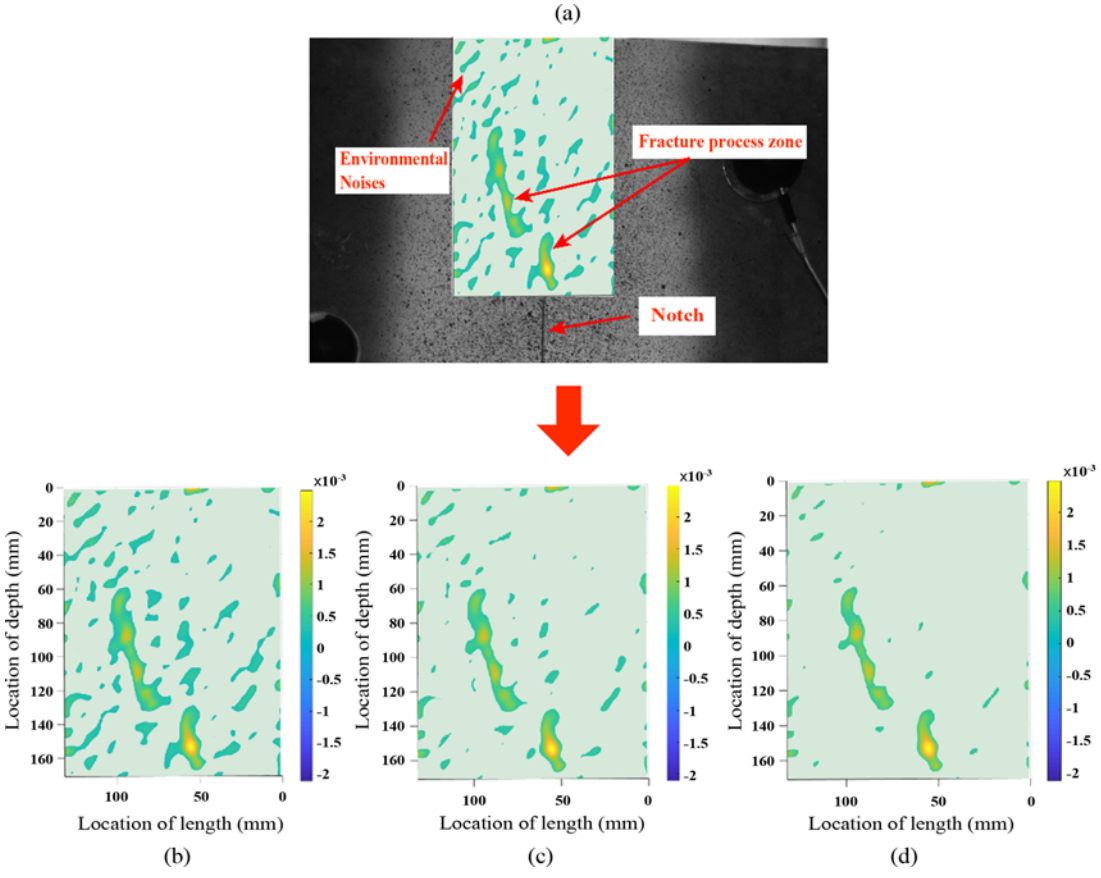

Fig. 13. Selection of Strain Threshold: (a) Horizontal Strain Contour, (b) T = 0.002, (c) T = 0.004, (d) T = 0.006

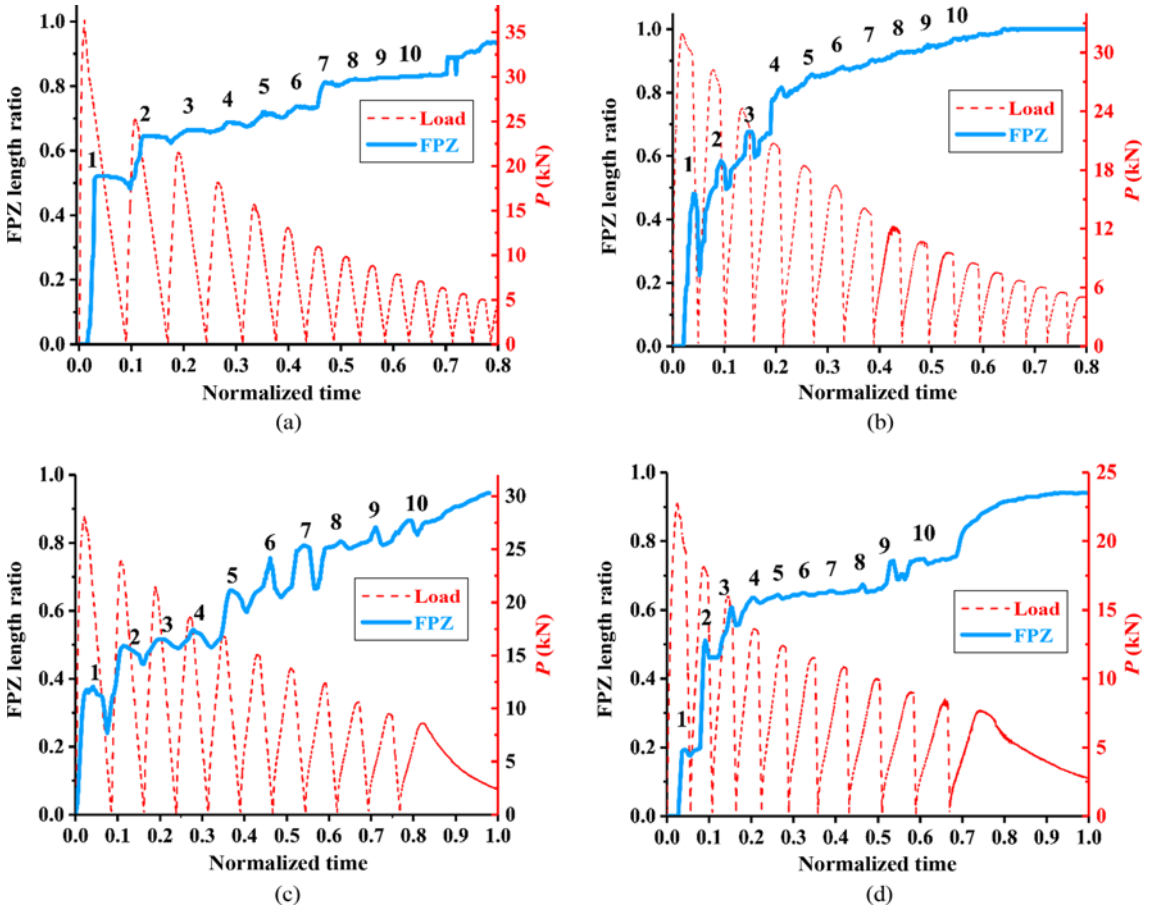

Fig. 14. Loading History and Variation in FPZ Length Ratio: (a) FDC-1, (b) FDC-2, (c) TDC-1, (d) TDC-2

the FPZ length changes only slightly as the load increases or decreases. This may be because at the early stage of deterioration, the development of FPZ is incomplete, and the micro-cracks are still developing, so the increase in FPZ is more significant. With the increase of the loading cycle, the micro-cracks develop and produce more permanent deformation, so the change of FPZ during unloading decreases.

As discussed above, it was found that the influence of loading rate on the post-peak residual bearing capacity is in sharp contrast with that on the maximum load. Furthermore, the results showed that the specimens with higher bearing capacity seem to have larger residual stiffness, dissipation energy, and recovery rate. These indicate that the difference of bearing capacity after peak may be related to the development degree of internal cracks. In the observation of FPZ length, some related phenomena were found. First of all, it can be noted from Fig. 14 that when the load reaches its peak value for the first time, the specimens with the higher loading rate, namely FDC-1 and TDC-1, have larger FPZ lengths. The specimens with larger FPZ length are transformed into those with lower residual bearing capacity in the post-peak stage, namely FDC-1 and TDC-2. This result is consistent with the normalized modulus results, which show that the specimens with lower residual bearing capacity have lower residual stiffness, more developed internal cracks, and the larger FPZ length also confirms this view.

Table 3. Reduction of FPZ Length Ratio after Unloading Procedure

Cycles	FDC-1	FDC-2	TDC-1	TDC-2
1	0.04	0.26	0.14	0.04
2	0.02	0.09	0.05	0.04
3	0.01	0.08	0.03	0.05
4	0.01	0.03	0.05	0.02

On the other hand, for larger dissipation energy and CMOD reversibility, which are parameters related to the unloading process, the corresponding phenomena can be found in the contraction of FPZ during the unloading process. It was found that the FPZ has a larger retraction rate during unloading for the specimens with higher residual bearing capacity. Table 3 shows the variation of the length ratio of FPZ in the first four loading cycles corresponding to the curve in Fig. 14. It can be seen that the FPZ length reduction of FDC-2 is much higher than FDC-1, which shows that the FPZ reversibility of FDC-2 is better than that of FDC-1. The same situation occurs in three-graded concrete. The dissipated energy, cyclic modulus, and CMOD reversibility of TDC-1 are higher, while the FPZ length ratio of TDC-1 decreases much more than TDC-2 during unloading. From Figs. 14(b) and 14(c), it can be

seen that the FPZ length of these two specimens decreases more dramatically after unloading in the previous cycles. In contrast, for the specimens with a lower load recovery rate, the length of FPZ almost does not change during unloading, and the propagation of FPZ presents a step-wise mode. It shows that the damage of concrete is more irreversible in these specimens, and the plastic damage of concrete in the process zone accounts for a larger proportion. From the view of these results mentioned above, it can be determined that the post-peak mechanical behavior of specimens with higher residual bearing capacity is significantly different and has a great relationship with the development of cracks. This proves the influence of crack development on the mechanical response of the structure.

4. Conclusions

The post-peak responses under cyclic loading of dam concrete beams were detailed in this paper. For different loading rates, two groups of tests were carried out on dam concrete. The results of this paper further revealed the mechanism of crack growth and closure, stiffness degradation, and cyclic energy consumption during the loading and unloading process of dam concrete, which is helpful to fracture mechanics models reflecting the loading and unloading process.The dynamic analysis of the FPZ development under cyclic load was realized by using DIC. The following conclusions can be drawn from this research work.

1. The P-CMOD relationships indicated that the maximum load-carrying capacity of concrete increased significantly with the loading rate, which is generally found in previous studies. However, the influence of loading rate on the post-peak residual bearing capacity is in sharp contrast with that on the maximum load, which was ignored in previous studies.
2. Different parameters, including the cyclic modulus, dissipated energy, and CMOD reversibility, were used to analyze dam concrete's post-peak behavior. The results show that the specimens with higher post-peak bearing capacity have an obviously different response in the post-peak field, which have higher residual stiffness, higher dissipation energy, and higher CMOD reversibility under cyclic loading.
3. There is a corresponding relationship between the FPZ length and the parameters obtained above. The higher residual stiffness indicates limited crack development in the specimen, which was confirmed by the observation of FPZ length. The results showed that FPZ developed more slowly with higher residual stiffness. For larger dissipation energy and CMOD reversibility, which are parameters related to the unloading process, the corresponding phenomena can be found in the contraction of FPZ during the unloading process. It was noticed that the FPZ has a more significant retraction rate during unloading for the specimens with higher residual bearing capacity.
4. The post-peak mechanical behavior of specimens with higher residual bearing capacity has a great relationship with the development of cracks. It was also suggested that more attention should be paid to the relationship between FPZ length and residual bearing capacity under cyclic load in future research.

Acknowledgments

The research is based upon the work supported by the Natural Science Foundation for Excellent Young Scholars of Jiangsu Province (Grant No. BK20190075); National Natural Science Foundation of China (Grant No. 51979090); Young Elite Scientists Sponsorship Program by China Association for Science and Technology (Grant No. 2017QNRC00).

Nomenclature

a = Crack length
a_0 = Initial crack length
a_c = Critical crack length
$CMOD_0$ = CMOD at the reloading beginning
$CMOD_c$ = CMOD at the maximum load
$CMOD_{max}$ = CMOD at the peak load
$CMOD_{residual}$ = CMOD at the end of unloading
E_0 = Tangent modulus at the beginning
E_l = Secant modulus of the loading process
$E_{l,50}$ = Tangent modulus at 50% loading stage
E_{unl} = Secant modulus of the unloading process
$E_{unl,50}$ = Tangent modulus at 50% unloading stage
exx = Horizontal strain
h = The height of the beam
K_{ini} = Initial fracture toughness
K_{un} = Critical fracture toughness
P_u = The maximum load
S = The span of the beam
T = Strain threshold
t = The thickness of the beam
W_i = The dissipated energy of the i-th loading cycle
α = Crack height ratio
β = Span-height ratio

ORCID

Xudong Chen https://orcid.org/0000-0003-0534-6927

References

Ardito R, Maier G, Massalongo G (2008) Diagnostic analysis of concrete dams based on seasonal hydrostatic loading. *Engineering Structures* 30(11):3176-3185, DOI: 10.1016/j.engstruct.2008.04.008

ASTM C33 (2003) Standard specifications for concrete aggregates. ASTM C33, ASTM International, West Conshohocken, PA, USA

Bažant ZP, Gettu R (1992) Rate effects and load relaxation in static fracture of concrete. *ACI Materials Journal* 89(5):456-468

Bhattacharjee SS, Leger P (1993) Seismic cracking and energy dissipation in concrete gravity dams. *Earthquake Engineering & Structural*

Dynamics 22(11):991-1007, DOI: 10.1002/eqe.4290221106

Bhowmik S, Ray S (2019) An experimental approach for characterization of fracture process zone in concrete. *Engineering Fracture Mechanics* 211:401-419, DOI: 10.1016/j.engfracmech.2019.02.026

Cedolin L, Dei Poli S, Iori I (1983) Experimental determination of the fracture process zone in concrete. *Cement and Concrete Research* 13(4):557-567, DOI: 10.1016/0008-8846(83)90015-7

Choi S, Shah SP (1997) Measurement of deformations on concrete subjected to compression using image correlation. *Experimental Mechanics* 37(3):307-313, DOI: 10.1007/BF02317423

De Sortis A, Paoliani P (2007) Statistical analysis and structural identification in concrete dam monitoring. *Engineering Structures* 29(1):110-120, DOI: 10.1016/j.engstruct.2006.04.022

Deng Z, Li Q, Fu H (2008) Comparison between mechanical properties of dam and sieved concretes. *Journal of Materials in Civil Engineering* 20(4):321-326, DOI: 10.1061/(ASCE)0899-1561(2008)20:4(321)

Elices M, Rocco CG (2008) Effect of aggregate size on the fracture and mechanical properties of a simple concrete. *Engineering Fracture Mechanics* 75(13):3839-3851, DOI: 10.1016/j.engfracmech.2008.02.011

Fedele R, Maier G, Miller B (2005) Identification of elastic stiffness and local stresses in concrete dams by in situ tests and neural networks. *Structure and Infrastructure Engineering* 1(3):165-180, DOI: 10.1080/15732470500030513

Ghrib F, Tinawi R (1995) An application of damage mechanics for seismic analysis of concrete gravity dams. *Earthquake Engineering & Structural Dynamics* 24(2):157-173, DOI: 10.1002/eqe.4290240203

Ghuzlan KA, Carpenter SH (2006) Fatigue damage analysis in asphalt concrete mixtures using the dissipated energy approach. *Canadian Journal of Civil Engineering* 33(7):890-901, DOI: 10.1139/l06-032

Guinea GV, Pastor JY, Planas J, Elices M (1998) Stress intensity factor, compliance and CMOD for a general three-point-bend beam. *International Journal of Fracture* 89(2):103-116, DOI: 10.1023/A:1007498132504

Guo Y, Chen X, Li X, Li S, Guo S (2019) Experimental study on fracture behavior of three-graded concrete under cyclic loading after initial static loading. *Theoretical and Applied Fracture Mechanics* 103:102272, DOI: 10.1016/j.tafmec.2019.102272

Hu X, Duan K (2004) Influence of fracture process zone height on fracture energy of concrete. *Cement and Concrete Research* 34(8):1321-1330, DOI: 10.1016/j.cemconres.2003.12.027

Hu XZ, Wittmann FH (1992) Fracture energy and fracture process zone. *Materials and Structures* 25(6):319-326, DOI: 10.1007/BF02472590

Leger P, Venturelli J, Bhattacharjee SS (1993) Seasonal temperature and stress distributions in concrete gravity dams, Part 1: Modeling. *Canadian Journal of Civil Engineering* 20(6):999-1017, DOI: 10.1139/l93-131

Li ST, Chen X, Feng L, Zhang X, Fan X, Lu J (2019a) Experimental study on concrete fracture process zone using digital image correlation technique. *Journal of Testing and Evaluation* 49(2), DOI: 10.1520/JTE20180863

Li X, Chen X, Jivkov AP, Zhang J (2019b) 3D mesoscale modeling and fracture property study of rubberized self-compacting concrete based on uniaxial tension test. *Theoretical and Applied Fracture Mechanics* 104:102363, DOI: 10.1016/j.tafmec.2019.102363

Li Q, Deng Z, Fu H (2004) Effect of aggregate type on mechanical behavior of dam concrete. *ACI Materials Journal* 101(6):483-492

Li ST, Fan XQ, Chen XD, Liu SS, Guo YZ (2020) Development of fracture process zone in full-graded dam concrete under three-point bending by DIC and acoustic emission. *Engineering Fracture Mechanics* 230:106972, DOI: 10.1016/j.engfracmech.2020.106972

Mata J (2011) Interpretation of concrete dam behaviour with artificial neural network and multiple linear regression models. *Engineering Structures* 33(3):903-910, DOI: 10.1016/j.engstruct.2010.12.011

Miao S, Pan PZ, Yu P, Zhao S, Shao C (2020) Fracture analysis of Beishan granite after high-temperature treatment using digital image correlation. *Engineering Fracture Mechanics* 225:106847, DOI: 10.1016/j.engfracmech.2019.106847

Mihashi H, Nomura N, Niiseki S (1991) Influence of aggregate size on fracture process zone of concrete detected with three dimensional acoustic emission technique. *Cement and Concrete Research* 31:737-744, DOI: 10.1016/0008-8846(91)90168-H

Nomura N, Mihashi H, Izumi M (1991) Correlation of fracture process zone and tension softening behavior in concrete. *Cement and Concrete Research* 21(4):545-550, DOI: 10.1016/0008-8846(91)90104-P

Poissant J, Barthelat F (2010) A novel "subset splitting" procedure for digital image correlation on discontinuous displacement fields. *Experimental Mechanics* 50(3):353-364, DOI: 10.1007/s11340-009-9220-2

Reinhardt HW, Cornelissen HAW (1984) Post-peak cyclic behaviour of concrete in uniaxial tensile and alternating tensile and compressive loading. *Cement and Concrete Research* 14(2):263-270, DOI: 10.1016/0008-8846(84)90113-3

Ren Q, Xu L, Wan Y (2007) Research advance in safety analysis methods for high concrete dam. *Science in China Series E: Technological Sciences* 50(1):62-78, DOI: 10.1007/s11431-007-6008-4

Safavizadeh SA, Kim YR (2017) DIC technique to investigate crack propagation in grid-reinforced asphalt specimens. *Journal of Materials in Civil Engineering* 29(6):04017011

Saouma VE, Broz JJ, Brühwiler E, Boggs HL (1991) Effect of aggregate and specimen size on fracture properties of dam concrete. *Journal of Materials in Civil Engineering* 3(3):204-218, DOI: 10.1061/(ASCE)0899-1561(1991)3:3(204)

Shah SP (1990) Determination of fracture parameters (K_{Ic}^{s} and $CTOD_c$) of plain concrete using three-point bend tests. *Materials and Structures* 23(6):457-460, DOI: 10.1007/BF02472029

Skarżyński Ł, Tejchman J (2013) Experimental investigations of fracture process using DIC in plain and reinforced concrete beams under bending. *Strain* 49(6):521-543

Song J, Gu C, Su H, Gu H, Huang X (2016) Observed displacement data-based identification method of structural damage in concrete dam. *Engineering Failure Analysis* 66:202-211, DOI: 10.1016/j.engfailanal.2016.04.013

Sutton MA, Turner JL, Bruck HA, Chao TA (1991) Full-field representation of discretely sampled surface deformation for displacement and strain analysis. *Experimental Mechanics* 31:168-177, DOI: 10.1007/BF02327571

Swartz SE, Go CG (1984) Validity of compliance calibration to cracked concrete beams in bending. *Experimental Mechanics* 24(2):129-134, DOI: 10.1007/BF02324995

Tatin M, Briffaut M, Dufour F, Simon A, Fabre JP (2015) Thermal displacements of concrete dams: Accounting for water temperature in statistical models. *Engineering Structures* 91:26-39, DOI: 10.1080/15732470500030513

Tong W (1997) Detection of plastic deformation patterns in a binary aluminum alloy. *Experimental Mechanics* 37(4):452-459, DOI: 10.1007/BF02317313

Wang CC, Deng JM, Ateshian GA, Hung CT (2002) An automated approach for direct measurement of two-dimensional strain distributions within articular cartilage under unconfined compression. *Journal of Bimechanical Engineering* 124(5):557-567, DOI: 10.1115/1.1503795

Wecharatana M, Shah SP (1983) Predictions of non-linear fracture process zone in concrete. *Journal of Engineering Mechanics* 109(5):1231-1246, DOI: 10.1061/(ASCE)0733-9399(1983)109:5(1231)

World Commission on Dams (2000) Dams and development: A new framework for decision-making. Earthscan, London, UK, 75-293

Wu K, Chen B, Yao W (2001) Study of the influence of aggregate size distribution on mechanical properties of concrete by acoustic emission technique. *Cement and Concrete Research* 31:919-923, DOI: 10.1016/S0008-8846(01)00504-X

Wu Z, Rong H, Zheng J, Xu F, Dong W (2011) An experimental investigation on the FPZ properties in concrete using digital image correlation technique. *Engineering Fracture Mechanics* 78(17):2978-2990, DOI: 10.1016/j.engfracmech.2011.08.016

Xu S, Reinhardt HW (1999) Determination of double-K criterion for crack propagation in quasi-brittle materials, Part II: Analytical evaluating and practical measuring methods for three-point bending notched beams. *International Journal of Fracture* 98(2):151-177, DOI: 10.1023/A:1018740728458

Zhang XX, Ruiz G, Yu RC, Tarifa M (2009) Fracture behaviour of high-strength concrete at a wide range of loading rates. *International Journal of Impact Engineering* 36(10-11):1204-1209, DOI: 10.1016/j.ijimpeng.2009.04.007